EDGE ARTICLE

Check for updates

Polyoxometalate condensation and transformation mediated by adaptive coordination-assembled molecular flasks†

Li-Xuan Cai, [ID] ac Yu-Hang Hu, ab Li-Peng Zhou, [ID] ac Pei-Ming Cheng, a Xiao-Qing Guo, a Yi-Tsu Chan [ID] d and Qing-Fu Sun [ID] *ac

Here we report polyoxometalate (POM) condensation or transformation reactions mediated by adaptive coordination-assembled molecular flasks. Addition of Na_2SiO_3 to the $(Mo_6O_{19})_2 \subset \mathbf{1} \cdot (NO_3)_8$ complex containing Lindquist-type clusters as guests leads to the formation of a new $(SiMo_{12}O_{40}) \subset \mathbf{2} \cdot (NO_3)_8$ host–guest complex, where the *in situ* generated Keggin-type cluster served as a trigger for the host transformation from cage **1** to isomeric bowl **2**. Conversion from **1** to **2** driven by the *in situ* condensation was found to be 27.5-fold faster than the direct templation with independently prepared $SiMo_{12}O_{40}{}^{4-}$. As a comparison, cage **1** was noticed to bind only one $W_6O_{19}{}^{2-}$ cluster in its cavity, and the formation of $(W_{10}O_{32}) \subset \mathbf{2} \cdot (NO_3)_8$ as the main product and $(SiW_{12}O_{40}) \subset \mathbf{2} \cdot (NO_3)_8$ as the minor host–guest complex was observed when it was used for the above condensation reaction, highlighting the crucial role of encapsulation in cavity-confined POM transformations. The reaction processes and the final structure of all the new host–guest complexes have been investigated by NMR, ESI-TOF-MS and SCXRD. Our findings not only showcase a unique example of inorganic-reaction-driven responsive supramolecular system, but also provide a new approach for the preparation of functional POMs⊂cage composite materials.

Introduction

Enzymes are biological catalysts with substrate-binding cavities that exhibit conformational dynamics and rich active sites, essential for efficient catalysis.[1–3] Inspired by these natural systems, scientists have developed coordination molecular containers based on supramolecular interactions to mimic enzyme functionality. The confined spaces of coordination-assembled cages, often referred to as 'molecular flasks', provide unique local microenvironments that allow for the encapsulation of guest molecules and endow them with reactivity distinctly different from the bulk solvent.[4–12] The tailored pockets of molecular flasks play a vital role in cage-promoted reactions through three major factors: preorganization and proximity of substrates to yield an unusual regioselectivity,[13,14] local concentration enrichment to accelerate reactions,[15,16] and

reaction intermediate stabilization to lower the energy and enthalpy barrier.[17–19] Despite extensive research on constructing stimuli-responsive supramolecular hosts with adaptive confined cavities,[20–34] examples of using such adaptive hosts as molecular flasks for inorganic chemical transformations remain scarce.

Polyoxometalates (POMs) are a well-known class of inorganic compounds that have shown wide-spread applications in diverse fields.[35–39] In nature, polyoxomolybdates can be stored in a cage-like Mo-storage protein (MoSto) from *Azotobacter vinelandii*.[40–42] Biological protein pockets are able to engineer condensation processes and stabilize the resulting fragile POM species by shielding against hydrolysis.[43] In laboratory, POMs are usually generated using bottom-up synthetic approaches, through acidic condensation of tetraoxometalates $MO_4{}^{2-}$ (M = Mo, W *etc.*), the outcome of which is very sensitive to synthetic variables, such as the pH, ionic strength, concentration *etc.*[44,45] POM transformation can happen by adjusting the solution conditions or by modifying the structural "vacancy" sites of lacunary POMs.[46] Although an artificial encapsulation approach has been demonstrated by installing POM anions into host systems *via* non-covalent and specific interactions,[47–59] the condensation or transformation of POM guests inside discrete adaptive coordination cages has been seldom targeted so far.

In our previous reports,[34,60,61] a mitosis-like host transformation from Pd_4L_2 cage **1** to a unique conjoined Pd_6L_3 twin-

aState Key Laboratory of Structural Chemistry, Fujian Institute of Research on the Structure of Matter, Chinese Academy of Sciences, Fuzhou 350002, P. R. China. E-mail: qfsun@fjirsm.ac.cn

bCollege of Chemistry and Materials Science, Fujian Normal University, Fuzhou 350007, P. R. China

cUniversity of Chinese Academy of Sciences, Beijing, 100049, P. R. China

dDepartment of Chemistry, National Taiwan University, Taipei 10617, Taiwan

cage **3** has been observed (Scheme 1A), driven by an organic self-coupling dimerization reaction of *ortho*-quinone methide precursors. Here we present the cavity-confined syntheses of Keggin-type POM clusters ($SiM_{12}O_{40}^{4-}$, M = Mo) from Lindquist-type $Mo_6O_{19}^{2-}$ precursors and SiO_3^{2-}, which exert the induced-fit power to force the structural conversion from cage **1** to isomeric bowl **2** (Scheme 1B). The same conversion also proceeds, but at a much slower rate, *via* the direct templating of independently made $SiMo_{12}O_{40}^{4-}$. As a comparison, the reaction of the other Lindqvist-type $W_6O_{19}^{2-}$ cluster with SiO_3^{2-} mediated by cage **1** led to not only Keggin-type $SiW_{12}O_{40}^{4-}$ but also $W_{10}O_{32}^{4-}$, both also accompanied by the induced-fit cage-to-bowl transformation. These POM synthesis reactions mediated by adaptive cages have been thoroughly investigated by IR, UV-vis, NMR, ESI-TOF-MS, and SCXRD.

Results and discussion

Cage **1**·$(NO_3)_{12}$ and $(Mo_6O_{19})_2 \subset 1 \cdot (NO_3)_8$ were synthesized according to our previous work (Fig. S1–S4†).[60,61] The optimized structure of $(Mo_6O_{19})_2 \subset 1 \cdot (NO_3)_8$ was simulated using molecular mechanical modeling (Fig. S5†). Surprisingly, when 1 equiv. of Na_2SiO_3 was added into the aqueous solution of $(Mo_6O_{19})_2 \subset 1 \cdot (NO_3)_8$, a dramatic ^1H NMR change was observed after heating at 70 °C for 12 h, accompanied by the darkening of the pale-yellow solution (Fig. 1, S6 and S7†). Two sets of protons signals consisting of 12 aromatic signals were observed after the
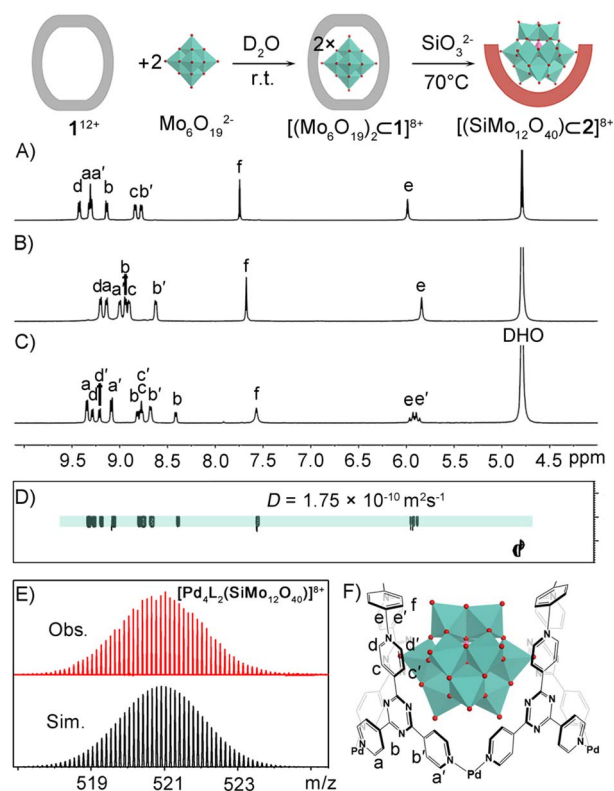

Fig. 1 Synthesis of the Keggin-type $SiMo_{12}O_{40}^{4-}$ anion within the adaptive cage. ^1H NMR spectra (400 M, D_2O, 298 K) of (A) **1**·$(NO_3)_{12}$, (B) $(Mo_6O_{19})_2 \subset 1 \cdot (NO_3)_8$, and (C) $(SiMo_{12}O_{40}) \subset 2 \cdot (NO_3)_8$ after heating the solution of $(Mo_6O_{19})_2 \subset 1 \cdot (NO_3)_8$ at 70 °C with Na_2SiO_3 for 12 h. (D) ^1H DOSY spectrum of $(SiMo_{12}O_{40}) \subset 2 \cdot (NO_3)_8$, and (E) ESI-TOF-MS of $(SiMo_{12}O_{40}) \subset 2 \cdot (NO_3)_8$, showing the observed and simulated isotopic patterns of the +8 peak; (F) the chemical structure of $(SiMo_{12}O_{40}) \subset 2 \cdot (NO_3)_8$.
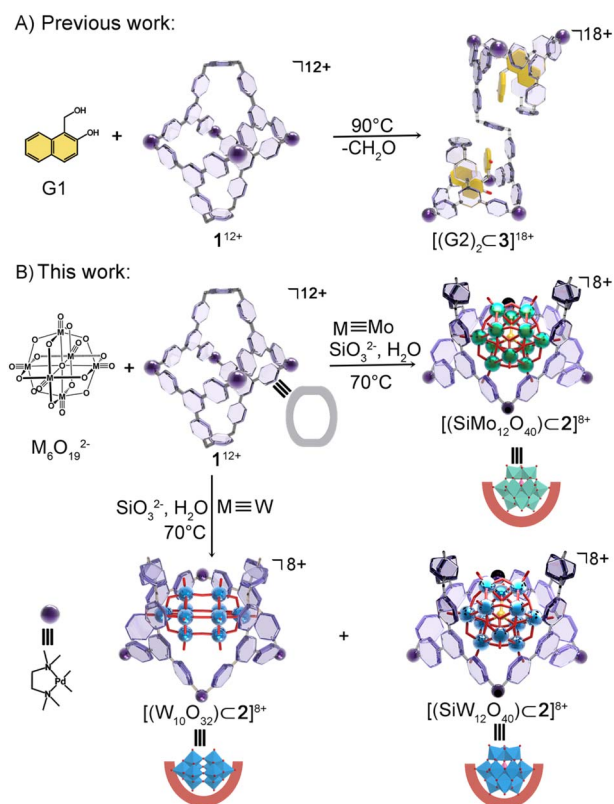
Scheme 1 (A) Organic self-coupling dimerization reaction triggered cage to twin-cage transformation. (B) Inorganic POM condensation reaction induced cage to bowl transformations.

reaction. The resonances of H_e in the CH_2 groups of the ligand (L) split into two doublets, along with a new set of splitting signals of H_d and H_c in the pyridinium group, all of which experienced two different magnetic environments. The DOSY spectrum shows that all the new signals have the same diffusion coefficient ($D = 1.75 \times 10^{-10}$ m^2 s^{-1}, Fig. 1D and S8†), different from that of $(Mo_6O_{19})_2 \subset 1 \cdot (NO_3)_8$ ($D = 2.43 \times 10^{-10}$ m^2 s^{-1}, Fig. S3†). The host–guest complex was characterized by high-resolution ESI-TOF-MS (Fig. 1E, S9 and S10†). Highly resolved +8 peaks observed at $m/z = 520.9201$ could be assigned to $[Pd_4L_2(SiMo_{12}O_{40})]^{8+}$. It is noted that the ^1H NMR of the inclusion complex $(Mo_6O_{19})_2 \subset 1 \cdot (NO_3)_8$ had almost no change even after heating at 70 °C for three days (Fig. S11†). Based on the above results, we inferred that a new POM species, $SiMo_{12}O_{40}^{4-}$, was formed in the system by the condensation of $Mo_6O_{19}^{2-}$ and SiO_3^{2-}, accompanied by the structural transformation of cage **1**.

Yellow block crystals suitable for SCXRD were obtained by slow evaporation of an aqueous solution of the host–guest complex (Fig. S46†). The inclusion complex crystallized in a hexagonal crystal system with the $P6_3$ space group. Remarkably, the crystal structure reveals that the Pd_4L_2-type cage **1** transformed into a structural isomer known as bowl **2**, benefited by the semirigid feature of the ligand with flexible *p*-

xylene linkers. A single Keggin-type α-$SiMo_{12}O_{40}^{4-}$ anion is tightly accommodated in the cavity of bowl-shaped host structure **2** (Fig. 2A). Multiple hydrogen bonding interactions between the *p*-xylene group and $SiMo_{12}O_{40}^{4-}$ (C–H···O=Mo), with distances ranging from 2.3778(1) to 2.9933(1) Å, were observed in the structure (Fig. S50†). Independent gradient model (IGM) analysis provides a visual depiction of the noncovalent bonding interactions (Fig. 2B and S48†), from which we inferred that the $SiMo_{12}O_{40}^{4-}$ anion is stabilized in the cavity by electrostatic and anion–π interactions as well as multiple intermolecular hydrogen bonding interactions. Additionally, in the crystal packing, three host–guest complexes aggregate into a trimer *via* π–π interactions between *p*-xylene and TPT panels (center-to-center distances: 3.6822(3)–3.8283(2) Å) (Fig. S50†).

The bowl **2** skeleton adopts the C_{2v} molecular symmetry (Fig. 2C), in contrast to the D_{2d}-symmetry of cage **1**, which aligns well with the NMR analysis. The cavity volume of bowl **2** was calculated to be *ca.* 963 Å^3 using MoloVol calculations based on the crystal structure (Fig. 2C and S52†),[62] which is larger than that of cage **1** (*ca.* 914 Å^3). This difference explains why the large-sized $SiMo_{12}O_{40}^{4-}$ anion is encapsulated by bowl **2** rather than cage **1**. According to Rebek's "55% rule",[63] optimal binding between the host and guest can be expected when the occupancy factor falls within the range 0.55 ± 0.09. The $SiMo_{12}O_{40}^{4-}$ anion has a maximum size of approximately 10.4 Å and a molecular volume of *ca.* 658 Å^3 (Fig. S53†). The occupancy factor of the bowl-cavity space by $SiMo_{12}O_{40}^{4-}$ is *ca.* 68%, smaller than that (72%) in the cage-cavity, which makes it more suitable for the optimal binding than **1**. Therefore, shape complementarity between Keggin-type $SiMo_{12}O_{40}^{4-}$ and the

bowl complex **2** drives the supramolecular structural transformation.

To shed light on the POM condensation induced-fit cage-to-bowl transformation mechanism, independently prepared $(TBA)_4SiMo_{12}O_{40}$ ($TBA = [(n\text{-}C_4H_9)_4N]^+$) was treated with $\mathbf{1}\cdot(NO_3)_{12}$ in D_2O solution. As observed in the ^1H NMR spectra, cage **1** cannot encapsulate the Keggin-type $SiMo_{12}O_{40}^{4-}$ in the cavity. Time-dependent ^1H NMR spectra with heating were collected to monitor the solution of $(Mo_6O_{19})_2 \subset \mathbf{1}\cdot(NO_3)_8$ after adding 1 equiv. of Na_2SiO_3, as well as the solution containing $SiMo_{12}O_{40}^{4-}$ and cage **1** (Fig. 3 and S12–S15†). Upon heating at 70 °C, signals assignable to the host–guest complex $(SiMo_{12}O_{40}) \subset \mathbf{2}\cdot(NO_3)_8$ gradually evolved, implying the simultaneous POM condensation and induced-fit cage transformation. For the *in situ* POM condensation driven cage-to-bowl conversion, over 92% transformation from $(Mo_6O_{19})_2 \subset \mathbf{1}\cdot(NO_3)_8$ to $(SiMo_{12}O_{40}) \subset \mathbf{2}\cdot(NO_3)_8$ was observed within 12 h. In sharp contrast, only 61% conversion for $SiMo_{12}O_{40}^{4-}$-induced structural transformation was observed even after heating at 70 °C for 8 d. Based on pseudo-first order reaction kinetics, a 27.5-fold higher rate constant of in situ-POM-condensation driven cage-to-bowl transformation was estimated, compared to that driven by $SiMo_{12}O_{40}^{4-}$ (Fig. 3D).

We also examined a similar condensation process with another Lindqvist $W_6O_{19}^{2-}$ cluster. Host–guest NMR titration experiments and ESI-TOF-MS revealed that only one $W_6O_{19}^{2-}$ cluster could be trapped in the cavity of **1** (Fig. S16–S20†). Then we wondered whether the reaction of $(TBA)_2W_6O_{19}$ and Na_2SiO_3 in the presence of $\mathbf{1}\cdot(NO_3)_{12}$ could also produce a similar Keggin-type product. The solution of 1 equiv. of Na_2SiO_3 and 2 equiv. of $W_6O_{19}^{2-}$ with $\mathbf{1}\cdot(NO_3)_{12}$ was heated for 15 h, resulting in a complicated ^1H NMR spectrum (Fig. S21†). The formation of the main product $(W_{10}O_{32}) \subset \mathbf{2}\cdot(NO_3)_8$, as well as the minor product $(SiW_{12}O_{40}) \subset \mathbf{2}\cdot(NO_3)_8$ was confirmed by ESI-TOF-MS (Fig. S22†). Observation of +4 and +3 charged species assigned to $(W_{10}O_{32}) \subset \mathbf{2}\cdot(NO_3)_8$ and $(SiW_{12}O_{40}) \subset \mathbf{2}\cdot(NO_3)_8$ provides the direct evidence. In addition, other signals attributable to $[Pd_4L_2(NO_3)_3(W_6O_{19})(HW_2O_7)(H_2O)_3]^{6+}$ and $[Pd_4L_2(NO_3)_5(W_6O_{19})(HW_2O_7)(H_2O)_3]^{4+}$ were observed in the mass spectrum. The cage-to-bowl transformation was then also checked with independently made $SiW_{12}O_{40}^{4-}$. Time-dependent ^1H NMR spectra of $\mathbf{1}\cdot(NO_3)_{12}$ and 1 equiv. of $SiW_{12}O_{40}^{4-}$ with heating at 70 °C exhibit 27% yield of clean $(SiW_{12}O_{40}) \subset \mathbf{2}\cdot(NO_3)_8$ (Fig. S23†) without the formation of other POM species. ESI-TOF-MS analysis of $(SiW_{12}O_{40}) \subset \mathbf{2}\cdot(BF_4)_8$ revealed a clear series of multivalent signals assignable to $[Pd_4L_2(BF_4)_nSiW_{12}O_{40}]^{8-n}$ ($n = 0$–4) (Fig. S24†). These results indicate that the full-encapsulation of the small POM precursors inside the cage cavity is crucial for efficient condensation reactions.

Previous reports have shown that the rapid transformation of $W_6O_{19}^{2-}$ to $W_{10}O_{32}^{4-}$ occurs when water is added to a methanolic solution containing $W_6O_{19}^{2-}$.[64,65] Thus the transformation of $W_6O_{19}^{2-}$ without SiO_3^{2-} was also examined in our system (Fig. 4A). When 2 equiv. of the $W_6O_{19}^{2-}$ anion was added to the H_2O solution of $\mathbf{1}\cdot(NO_3)_{12}$ and heated at 70 °C, ^1H NMR spectra show the disappearance of the starting material along
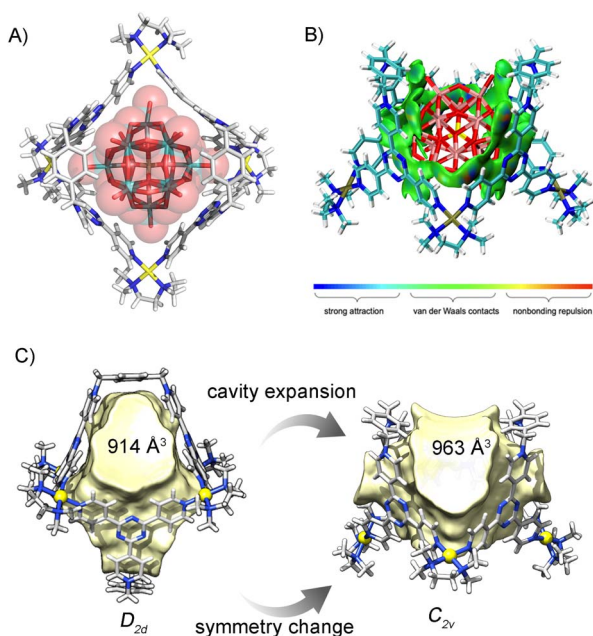

Fig. 2 (A) Crystal structure of $(SiMo_{12}O_{40}) \subset \mathbf{2}\cdot(NO_3)_8$. (B) Visualized intermolecular binding iso-surface between **2** and $SiMo_{12}O_{40}^{4-}$ (δg_{inter} = 0.003). (C) Cavity volumes of cage **1** and bowl **2** calculated using the MoloVol program based on the crystal structures.
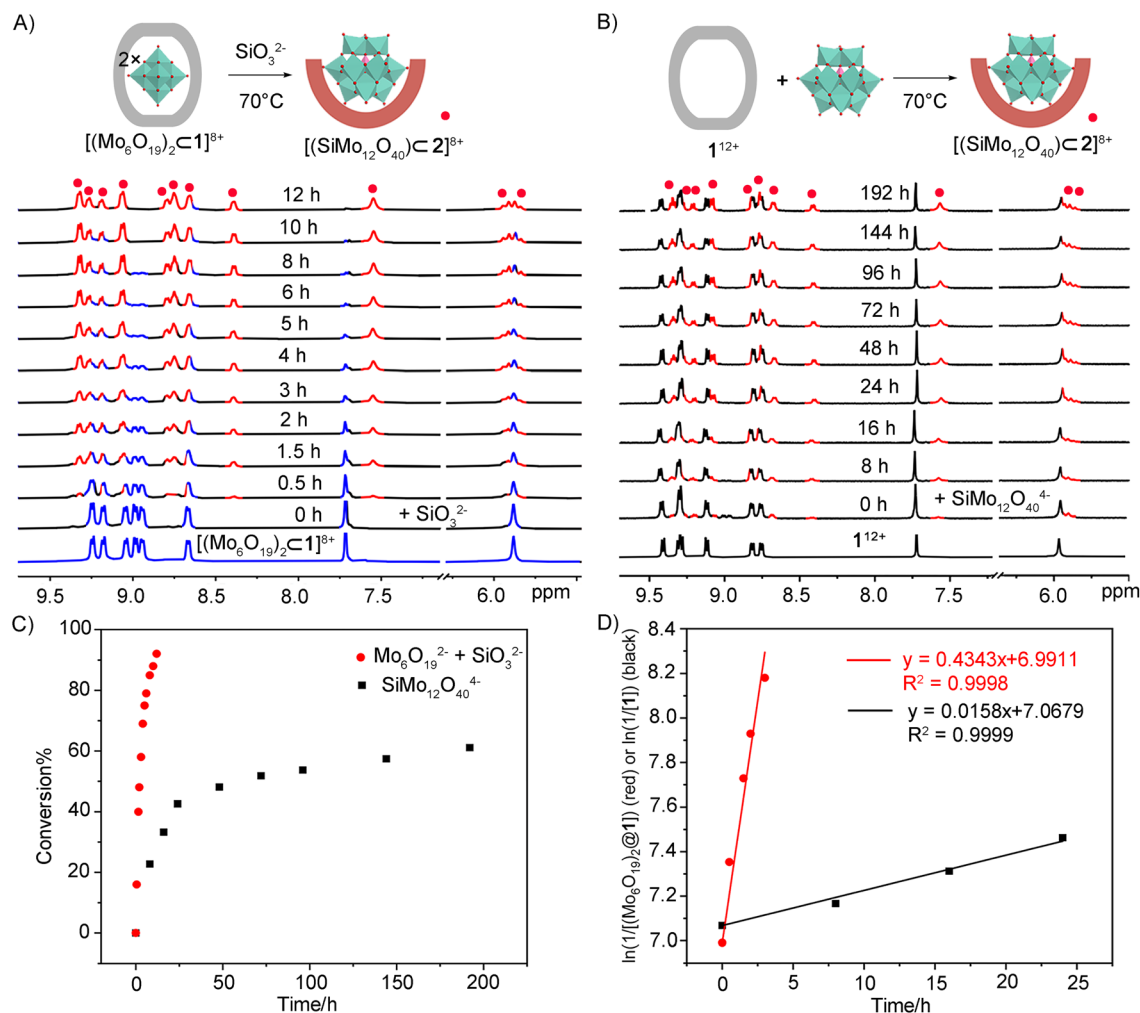
Fig. 3 Time-dependent ^1H NMR (400 M, D_2O, 298 K) for (A) $(Mo_6O_{19})_2 \subset 1 \cdot (NO_3)_8$ after adding 1 equiv. of Na_2SiO_3 and heating at 70 °C and (B) the $SiMo_{12}O_{40}^{4-}$ induced structural transformation from **1** to **2**. (C) Conversion and (D) pseudo-first-order kinetic plots for the above two cage transformation reactions.

with the coinstantaneous evolvement of two sets of new species (Fig. 4B and C). ESI-TOF-MS reveals the formation of new host–guest complexes assignable to $(W_{10}O_{32}) \subset Pd_4L_2$ (Fig. 4D, S27 and S28†). ^1H NMR spectra of $1 \cdot (NO_3)_{12}$ with the addition of independently prepared $(TBA)_2W_{10}O_{32}$ showed almost identical NMR spectra (Fig. S34†). Based on the NMR of $1 \cdot (NO_3)_{12}$ and $(TBA)_4W_{10}O_{32}$ (Fig. S29–S32†), along with the symmetry of the cage and bowl, one set of signals is assigned to $(W_{10}O_{32}) \subset 1 \cdot (NO_3)_8$ and the other to $(W_{10}O_{32}) \subset 2 \cdot (NO_3)_8$. This is further supported by the ESI-TOF-MS analyses (Fig. S36†).

SCXRD provided direct proof of the structural transformation. After heating $W_6O_{19}^{2-}$ in the aqueous solution of $1 \cdot (NO_3)_{12}$ at 70 °C for 2 days, single crystals of $(W_{10}O_{32}) \subset 2 \cdot (NO_3)_8$ were obtained by slow vapor diffusion of THF into the system. X-ray structural analysis reveals a 1 : 1 host–guest complex, where a $W_{10}O_{32}^{4-}$ anion was encapsulated into the cavity of bowl **2** (Fig. 5A). The average diagonal Pd–Pd distances in the structure of $(W_{10}O_{32}) \subset 2 \cdot (NO_3)_8$ are 17.3563(34) Å and 19.3029(38) Å. IGM analysis revealed that electrostatic, anion–π interactions and multiple hydrogen bonds work together to

stabilize this host–guest complex (Fig. 5B and S49†). As the maximum size and the volume of $W_{10}O_{32}^{4-}$ are *ca.* 12.0 Å and 558 Å³, respectively, the occupancy factor of $W_{10}O_{32}^{4-}$ in the bowl-cavity of **2** is *ca.* 58%, compared to 61% in the cage cavity of **1** (Table S1†). $W_{10}O_{32}^{4-}$ also can be shape-matched well with the bowl-shape space of **2** and multiple non-covalent interactions drive the guest-reaction induced-fit structural transformation.

Crystallization of the $(SiW_{12}O_{40}) \subset 2 \cdot (NO_3)_8$ complex was also successful. In the crystal structure, the complex crystallized in the monoclinic crystal system with the $P2_1/n$ space group. One $SiW_{12}O_{40}^{4-}$ anion sits inside the bowl-shaped cage **2**, similar to $SiMo_{12}O_{40}^{4-}$ (Fig. 5C and D). IGM analysis confirmed similar non-covalent interactions in stabilizing this iso-structural host–guest complex as observed with $(SiMo_{12}O_{40}) \subset 2 \cdot (NO_3)_8$.

UV-vis absorption spectra also supported the POM synthesis driven supramolecular transformation processes (Fig. S37 and S38†). After heating the solution of the inclusion complex $(Mo_6O_{19})_2 \subset 1 \cdot (NO_3)_8$ at 70 °C with $NaSiO_3$ in H_2O, the structural conversion to $(SiMo_{12}O_{40}) \subset 2 \cdot (NO_3)_8$ was indicated by the
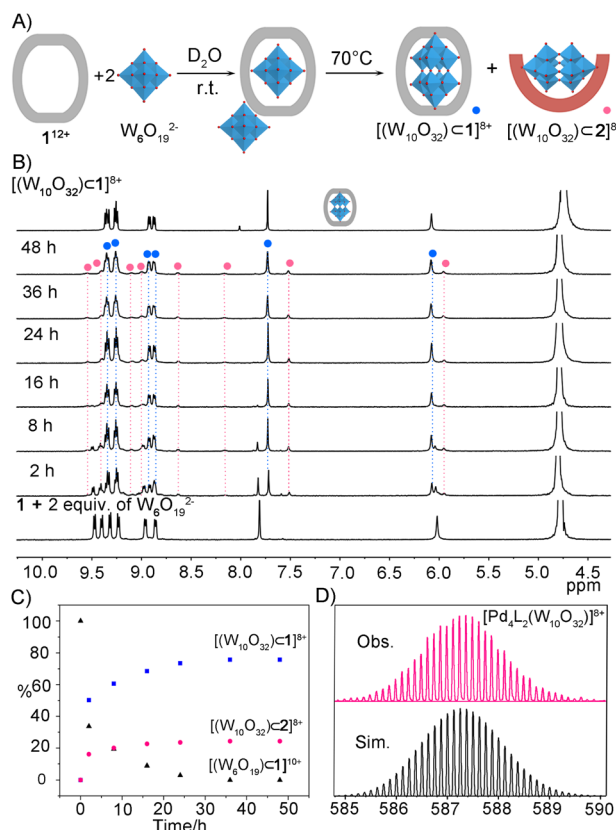
Fig. 4 (A) Structural transformation from cage **1** to bowl **2** induced by the $W_6O_{19}^{2-}$ conversion reaction and (B) time-dependent ^1H NMR (400 M, D_2O, 298 K) for $(W_6O_{19})_2 \subset 1 \cdot (NO_3)_8$ upon heating at 70 °C. (C) The corresponding conversion yield and (D) ESI-TOF-MS spectrum showing the observed and simulated isotopic patterns of the +8 peak of the resulting inclusion complex.

Fig. 5 The top view for the X-ray structure of inclusion complexes (A) $(W_{10}O_{32}) \subset 2 \cdot (NO_3)_8$, and (C) $(SiW_{12}O_{40}) \subset 2 \cdot (NO_3)_8$, showing the diagonal Pd–Pd distances. IGM analysis for (B) $(W_{10}O_{32}) \subset 2 \cdot (NO_3)_8$ and (D) $(SiW_{12}O_{40}) \subset 2 \cdot (NO_3)_8$ ($\delta g_{inter} = 0.003$). The color scale shows a range of interaction strengths: strong attraction (blue), weak contacts (green), and nonbonding repulsion (red).

appearance of a new absorption band tailing to the region until *ca.* 400 nm. In the IR spectra (Fig. S39†), the characteristic peaks of $\nu(Mo=O)$ and $\nu(O-Mo-O)$ for $(Mo_6O_{19})_2 \subset 1 \cdot (NO_3)_8$ were observed at 956 and 800 cm^{-1}, respectively, which disappeared when forming the new host–guest complex of $(SiMo_{12}O_{40}) \subset 2 \cdot (NO_3)_8$, along with new peaks at 945, 901, 795 cm^{-1} assignable to $SiMo_{12}O_{40}^{4-}$. As for the conversion from $W_6O_{19}^{2-}$ to $W_{10}O_{32}^{4-}$, new peaks in the region of 961–434 cm^{-1} corresponding to $W_{10}O_{32}^{4-}$ were observed after heating the sample of the mixture of $W_6O_{19}^{2-}$ (2 equiv.) and $1 \cdot (NO_3)_{12}$ (Fig. S40†). The peaks at 961, 893 and 804 cm^{-1} correspond to $\nu(W-O_t)$, $\nu(W-O_b-W)$, and $\nu(W-O_c-W)$ of the $[W_{10}O_{32}]^{4-}$ cluster, respectively.[48,66,67]

Plausible mechanisms were proposed for the POM condensation/transformation induced cage-to-bowl conversion. In the case of $Mo_6O_{19}^{2-}$, two precursors are encapsulated by the cavity of cage **1** and condensation happens after the addition of SiO_3^{2-}. The resulting $SiMo_{12}O_{40}^{4-}$ anion instigates the induced-fit transformation from cage **1** to bowl **2**. In fact, when $(TBA)_2$-Mo_6O_{19} was treated with Na_2SiO_3 and heated at 70 °C for 4 days as a control, no $SiMo_{12}O_{40}^{4-}$ anion was observed (Fig. S41†), suggesting the vital role of cage **1** in the synthesis of $SiMo_{12}O_{40}^{4-}$. Similarly, no $W_{10}O_{32}^{4-}$ or $SiW_{12}O_{40}^{4-}$ was observable by heating $(TBA)_2W_6O_{19}$ and Na_2SiO_3 at 70 °C in

H_2O/CH_3CN (v/v, 4/1) even for 4 days (Fig. S42†). Moreover, a remarkable stability of $SiMo_{12}O_{40}^{4-}$ hydrolytically protected within the bowl host was confirmed in water, as ^1H NMR witnessed negligible change for the $(SiMo_{12}O_{40}) \subset 2 \cdot (NO_3)_8$ complex even after standing at room temperature for one year (Fig. S44 and S45†).

Conclusions

In summary, we have discovered an induced-fit supramolecular transformation driven by *in situ* POM condensation reactions. Our work represents the first report on inorganic condensation reaction driven supramolecular structure transformation, which may provide new design principles for chemically fueled molecular machines. We also envision that efficient embedding of POMs into adaptive supramolecular hosts could be very promising for the development of functional hybrid materials.

Data availability

The data supporting this article have been included as part of the ESI.† Crystallographic data have been deposited at the CCDC under numbers 2360627, 2380035 and 2380036, and can be obtained from **https://www.ccdc.cam.ac.uk/structures/**.

Author contributions

Q.-F. S. and L.-X. C. conceived and designed this project. L.-X. C. carried out the synthesis, characterization, conducted the experiments and analyzed all the results. Y.-H. H. assisted with the synthesis. L.-P. Z. and Y.-T. C. performed the mass spectroscopy measurement. P.-M. C and X.-Q. G. contributed to the figure production. L.-X. C. and Q.-F. S. wrote the manuscript with input from all the authors.

Conflicts of interest

The authors declare no conflict of interest.

Acknowledgements

Notes and references

1 Y. Jin, Q. Zhang, Y. Zhang and C. Duan, *Chem. Soc. Rev.*, 2020, **49**, 5561–5600.

2 D. D. Boehr, R. Nussinov and P. E. Wright, *Nat. Chem. Biol.*, 2009, **5**, 789–796.

3 Z. Dong, Q. Luo and J. Liu, *Chem. Soc. Rev.*, 2012, **41**, 7890–7908.

4 C. J. Brown, F. D. Toste, R. G. Bergman and K. N. Raymond, *Chem. Rev.*, 2015, **115**, 3012–3035.

5 M. Yoshizawa, J. K. Klosterman and M. Fujita, *Angew. Chem., Int. Ed.*, 2009, **48**, 3418–3438.

6 E. G. Percastegui, T. K. Ronson and J. R. Nitschke, *Chem. Rev.*, 2020, **120**, 13480–13544.

7 C. J. Brown, F. D. Toste, R. G. Bergman and K. N. Raymond, *Chem. Rev.*, 2015, **115**, 3012–3035.

8 J. Guo, Y.-Z. Fan, Y.-L. Lu, S.-P. Zheng and C.-Y. Su, *Angew. Chem., Int. Ed.*, 2020, **59**, 8661–8669.

9 D. Liu, H. Ma, C. Zhu, F. Qiu, W. Yu, L.-L. Ma, X.-W. Wei, Y.-F. Han and G. Yuan, *J. Am. Chem. Soc.*, 2024, **146**, 2275–2285.

10 G. Wu, Y. Chen, S. Fang, L. Tong, L. Shen, C. Ge, Y. Pan, X. Shi and H. Li, *Angew. Chem., Int. Ed.*, 2021, **60**, 16594–16599.

11 R. L. Spicer, H. M. O'Connor, Y. Ben-Tal, H. Zhou, P. J. Boaler, F. C. Milne, E. K. Brechin, G. C. Lloyd-Jones and P. J. Lusby, *Chem. Sci.*, 2023, **14**, 14140–14145.

12 S. Matsuno, M. Yamashina, Y. Sei, M. Akita, A. Kuzume, K. Yamamoto and M. Yoshizawa, *Nat. Commun.*, 2017, **8**, 749.

13 M. Yoshizawa, M. Tamura and M. Fujita, *Science*, 2006, **312**, 251–254.

14 K. Iizuka, H. Takezawa and M. Fujita, *J. Am. Chem. Soc.*, 2023, **145**, 25971–25975.

15 W. Cullen, M. C. Misuraca, C. A. Hunter, N. H. Williams and M. D. Ward, *Nat. Chem.*, 2016, **8**, 231–236.

16 J. Jiao, Z. Li, Z. Qiao, X. Li, Y. Liu, J. Dong, J. Jiang and Y. Cui, *Nat. Commun.*, 2018, **9**, 4423.

17 K. Wang, J. H. Jordan, X. Y. Hu and L. Wang, *Angew. Chem., Int. Ed.*, 2020, **59**, 13712–13721.

18 Y. Fang, J. A. Powell, E. Li, Q. Wang, Z. Perry, A. Kirchon, X. Yang, Z. Xiao, C. Zhu, L. Zhang, F. Huang and H. C. Zhou, *Chem. Soc. Rev.*, 2019, **48**, 4707–4730.

19 H. Takezawa, K. Shitozawa and M. Fujita, *Nat. Chem.*, 2020, **12**, 574–578.

20 A. J. McConnell, C. S. Wood, P. P. Neelakandan and J. R. Nitschke, *Chem. Rev.*, 2015, **115**, 7729–7793.

21 W. Wang, Y.-X. Wang and H.-B. Yang, *Chem. Soc. Rev.*, 2016, **45**, 2656–2693.

22 O. Gidron, M. Jirasek, N. Trapp, M. O. Ebert, X. Zhang and F. Diederich, *J. Am. Chem. Soc.*, 2015, **137**, 12502–12505.

23 R. Zhu, J. Lubben, B. Dittrich and G. H. Clever, *Angew. Chem., Int. Ed.*, 2015, **54**, 2796–2800.

24 S.-P. Zheng, Y.-W. Xu, P.-Y. Su, C.-H. Liu, Y.-H. Huang, Y.-L. Lu, Z.-W. Wei, Z. Jiao, H.-S. Xu and C.-Y. Su, *Chin. Chem. Lett.*, 2024, **35**, 108477.

25 L.-L. Yan, L.-Y. Yao, M. Ng and V. W.-W. Yam, *J. Am. Chem. Soc.*, 2021, **143**, 19008–19017.

26 X.-R. Liu, P.-F. Cui, S.-T. Guo, Y.-J. Lin and G.-X. Jin, *J. Am. Chem. Soc.*, 2023, **145**, 8569–8575.

27 H. J. Yoon, J. Kuwabara, J. H. Kim and C. A. Mirkin, *Science*, 2010, **330**, 66–69.

28 S. Wang, T. Sawada, K. Ohara, K. Yamaguchi and M. Fujita, *Angew. Chem., Int. Ed.*, 2016, **55**, 2063–2066.

29 D. M. Wood, W. Meng, T. K. Ronson, A. R. Stefankiewicz, J. K. Sanders and J. R. Nitschke, *Angew. Chem., Int. Ed.*, 2015, **54**, 3988–3992.

30 A. Walther, I. Regeni, J. J. Holstein and G. H. Clever, *J. Am. Chem. Soc.*, 2023, **145**, 25365–25371.

31 R. Banerjee, S. Bhattacharyya and P. S. Mukherjee, *JACS Au*, 2023, **3**, 1998–2006.

32 K. Hema, A. B. Grommet, M. J. Bialek, J. Wang, L. Schneider, C. Drechsler, O. Yanshyna, Y. Diskin-Posner, G. H. Clever and R. Klajn, *J. Am. Chem. Soc.*, 2023, **145**, 24755–24764.

33 S. Wang, T. Sawada and M. Fujita, *Chem. Commun.*, 2016, **52**, 11653–11656.

34 P.-M. Cheng, L.-X. Cai, S.-C. Li, S.-J. Hu, D.-N. Yan, L.-P. Zhou and Q.-F. Sun, *Angew. Chem., Int. Ed.*, 2020, **59**, 23569–23573.

35 S. S. Wang and G. Y. Yang, *Chem. Rev.*, 2015, **115**, 4893–4962.

36 D.-L. Long, R. Tsunashima and L. Cronin, *Angew. Chem., Int. Ed.*, 2010, **49**, 1736–1758.

37 A. Dolbecq, E. Dumas, C. R. Mayer and P. Mialane, *Chem. Rev.*, 2010, **110**, 6009–6048.

38 D.-Y. Du, J.-S. Qin, S.-L. Li, Z.-M. Su and Y.-Q. Lan, *Chem. Soc. Rev.*, 2014, **43**, 4615–4632.

39 D. Ravelli, S. Protti and M. Fagnoni, *Acc. Chem. Res.*, 2016, **49**, 2232–2242.

40 B. Kowalewski, J. Poppe, U. Demmer, E. Warkentin, T. Dierks, U. Ermler and K. Schneider, *J. Am. Chem. Soc.*, 2012, **134**, 9768–9774.

41 D. Fenske, M. Gnida, K. Schneider, W. Meyer-Klaucke, J. Schemberg, V. Henschel, A.-K. Meyer, A. Knöchel and A. Müller, *ChemBioChem*, 2005, **6**, 405–413.

42 S. Brünle, M. L. Eisinger, J. Poppe, D. J. Mills, J. D. Langer, J. Vonck and U. Ermler, *Proc. Natl. Acad. Sci. U. S. A.*, 2019, **116**, 26497–26504.

43 C. Molitor, A. Bijelic and A. Rompel, *Chem. Commun.*, 2016, **52**, 12286–12289.

44 W. Xuan, A. J. Surman, Q. Zheng, D. L. Long and L. Cronin, *Angew. Chem., Int. Ed.*, 2016, **55**, 12703–12707.

45 M. Bugnola, R. E. Schreiber, Y. Kaufman, G. Leitus, L. J. W. Shimon and R. Neumann, *Eur. J. Inorg. Chem.*, 2019, **2019**, 482–485.

46 H. Liu, C.-Y. Song, R.-W. Huang, Y. Zhang, H. Xu, M.-J. Li, S.-Q. Zang and G.-G. Gao, *Angew. Chem., Int. Ed.*, 2016, **55**, 3699–3703.

47 Y. Wu, R. Shi, Y. L. Wu, J. M. Holcroft, Z. Liu, M. Frasconi, M. R. Wasielewski, H. Li and J. F. Stoddart, *J. Am. Chem. Soc.*, 2015, **137**, 4111–4118.

48 K. Uehara, K. Kasai and N. Mizuno, *Inorg. Chem.*, 2007, **46**, 2563–2570.

49 M. Han, J. Hey, W. Kawamura, D. Stalke, M. Shionoya and G. H. Clever, *Inorg. Chem.*, 2012, **51**, 9574–9576.

50 Y. Liu, C. Hu, A. Comotti and M. D. Ward, *Science*, 2011, **333**, 436–440.

51 D. Prochowicz, A. Kornowicz and J. Lewinski, *Chem. Rev.*, 2017, **117**, 13461–13501.

52 M. Stuckart and K. Y. Monakhov, *Chem. Sci.*, 2019, **10**, 4364–4376.

53 Q. Han, C. He, M. Zhao, B. Qi, J. Niu and C. Duan, *J. Am. Chem. Soc.*, 2013, **135**, 10186–10189.

54 M. A. Moussawi, M. Haouas, S. Floquet, W. E. Shepard, P. A. Abramov, M. N. Sokolov, V. P. Fedin, S. Cordier, A. Ponchel, E. Monflier, J. Marrot and E. Cadot, *J. Am. Chem. Soc.*, 2017, **139**, 14376–14379.

55 M. A. Moussawi, N. Leclerc-Laronze, S. Floquet, P. A. Abramov, M. N. Sokolov, S. Cordier, A. Ponchel, E. Monflier, H. Bricout, D. Landy, M. Haouas, J. Marrot and E. Cadot, *J. Am. Chem. Soc.*, 2017, **139**, 12793–12803.

56 C. Falaise, M. A. Moussawi, S. Floquet, P. A. Abramov, M. N. Sokolov, M. Haouas and E. Cadot, *J. Am. Chem. Soc.*, 2018, **140**, 11198–11201.

57 S.-B. Yu, Q. Qi, B. Yang, H. Wang, D.-W. Zhang, Y. Liu and Z.-T. Li, *Small*, 2018, **14**, 1801037.

58 X.-F. Li, S.-B. Yu, B. Yang, J. Tian, H. Wang, D.-W. Zhang, Y. Liu and Z.-T. Li, *Sci. China:Chem.*, 2018, **61**, 830–835.

59 M. Yan, X.-B. Liu, Z.-Z. Gao, Y.-P. Wu, J.-L. Hou, H. Wang, D.-W. Zhang, Y. Liu and Z.-T. Li, *Org. Chem. Front.*, 2019, **6**, 1698–1704.

60 L. X. Cai, S. C. Li, D. N. Yan, L. P. Zhou, F. Guo and Q. F. Sun, *J. Am. Chem. Soc.*, 2018, **140**, 4869–4876.

61 S.-C. Li, L.-X. Cai, L.-P. Zhou, F. Guo and Q.-F. Sun, *Sci. China:Chem.*, 2019, **62**, 713–718.

62 J. B. Maglic and R. Lavendomme, *J. Appl. Crystallogr.*, 2022, **55**, 1033–1044.

63 S. Mecozzi and J. Rebek Julius, *Chem.–Eur. J.*, 1998, **4**, 1016–1022.

64 M. T. Pope, *Heteropoly and isopoly oxometalates*, Springer, Berlin, 1983, p. 54.

65 P.-P. Shen, Y.-N. Chi, Z.-G. Lin and C.-W. Hu, *Inorg. Chem. Commun.*, 2013, **29**, 197–200.

66 W. G. Klemperer, Tetrabutylammonium Isopolyoxometalates, in *Inorganic Syntheses*, 1990, pp. 74–85.

67 H. Xu, Z. Li, B. Liu, G. Xue, H. Hu, F. Fu and J. Wang, *Cryst. Growth Des.*, 2010, **10**, 1096–1103.